Hindawi
Shock and Vibration
Volume 2020, Article ID 8871433, 17 pages
https://doi.org/10.1155/2020/8871433

Research Article

Incipient Fault Detection of Rolling Element Bearings Based on Deep EMD-PCA Algorithm

Huaitao Shi,[1] Jin Guo,[1] Zhe Yuan,[1] Zhenpeng Liu,[1] Maxiao Hou,[1] and Jie Sun[2]

[1]*School of Mechanical Engineering, Shenyang Jianzhu University, Shenyang, Liaoning 110168, China*
[2]*The State Key Laboratory of Rolling and Automation, Northeastern University, Shenyang, Liaoning 110819, China*

Correspondence should be addressed to Zhe Yuan; yuanzhe@sjzu.edu.cn

Received 23 July 2020; Revised 23 September 2020; Accepted 15 October 2020; Published 27 October 2020

Academic Editor: Changqing Shen

Due to the relatively weak early fault characteristics of rolling bearings, the difficulty of early fault detection increases. For unsolving this problem, an incipient fault detection method based on deep empirical mode decomposition and principal component analysis (Deep EMD-PCA) is proposed. In this method, multiple data processing layers are created to extract weak incipient fault features, and EMD is used to decompose the vibration signal. This method establishes an accurate data mode, which can improve the incipient fault detection capability. It overcomes the difficulties of incipient fault detection, in which weak fault features can be extracted from the background of strong noise. From a theoretical point of view, this paper proves that the Deep EMD-PCA method can retain more variance information and has a good early fault detection ability. The experiment results indicate that the detection rate of Deep EMD-PCA is about 85%, and the failure detection delay time is almost zero. The incipient faults of rolling element bearings can be detected accurately and timely by Deep EMD-PCA. The method effectively improves the accuracy and timeliness of fault detection under actual working conditions and has good practical application value.

1. Introduction

Rolling element bearings are one of the common mechanical components in rotating machinery, and their operating conditions often directly affect the performance of the entire machine [1–3]. It is vital to detect the incipient faults of rolling element bearings accurately and timely, which can prevent them from developing into a more serious fault, resulting in huge losses [4]. Vibration signal analysis is the main technique to diagnose a rolling bearing fault [5, 6]. The main challenges of incipient fault detection for rolling element bearings are as follows [7, 8]:

(1) The incipient features of the device are weak and insignificant, and the fault signal is often buried in a strong noise background. During the running process of the rolling element bearings, there is a large amount of amplitude interference noise in the signal

(2) Due to the harsh operating environment and limited field measurement conditions, the obtained signal has an impact interference signal

There are many incipient fault detection methods for rolling element bearings, which can be roughly divided into two methods based on model-driven and data-driven methods [9]. An incipient fault detection method based on analytical models requires modeling the system to analyze system faults [10, 11]. Due to the inaccuracy of the modeling, the detection performance of the system failure is reduced. Data-driven methods can effectively overcome these problems. The data collected by the system is analyzed by data-driven methods, to achieve the effect of incipient fault detection [12–14].

Signal decomposition methods are commonly used for vibration signals [15], including wavelet transform methods [16, 17] and empirical mode decomposition (EMD) methods [18–20]. The wavelet transform method cannot achieve adaptive decomposition because it is limited by the basis function. The EMD method is a common method for analyzing nonstationary, nonlinear vibration signals. However, due to the inclusion of some redundant information in the feature extraction process, the data dimension is high and the calculation efficiency is low.

Deep learning is one of the popular incipient detection methods [21, 22]. The commonly used deep learning incipient fault detection methods include Support Vector Machine (SVM) [23] and Convolutional Neural Networks (CNN) [24]. These methods can compress the signal to achieve dimensionality reduction. However, the computational strength of the model becomes larger, and the training speed of the system decreases in a large network structure.

A common fault detection method for removing data redundancy and reducing the data dimension is the principal component analysis (PCA) method [25–27]. The main idea is to project the high-dimensional data space into the low-dimensional principal component space [28]. However, due to the PCA method in the process of extracting the feature values, only a small number of principal elements are selected, resulting in the loss of information, and it is impossible to diagnose some weak fault features. The study [29] proposed a new data-driven method based on Deep PCA for incipient fault diagnosis. The method can decompose the fault information in a more detailed manner, obtain weak fault features, and achieve the effect of incipient fault diagnosis. But the PCA fault detection method cannot detect the vibration signal.

In order to solve the above problems, this paper proposes an incipient fault diagnosis method based on Deep EMD-PCA. Firstly, the EMD-PCA fault detection method is used to extract the effective information in the vibration signal and remove the noise information in the vibration signal. Secondly, the data is decomposed to obtain multiple subdatasets. Finally, each subdataset is analyzed, redundant information is removed, and weaker fault features will be mined to detect incipient faults in rolling element bearings. Deep EMD-PCA can mine the small fault information in the vibration signal and better detect the incipient fault problem compared with the traditional EMD-PCA fault diagnosis method. In the third part and the fourth part, the fault detection capability of the method is proved from both theoretical and experimental aspects.

The main structure of this paper is as follows. The second part introduces the basic theoretical knowledge of EMD and PCA. The third part presents the fault detection method based on Deep EMD-PCA and proves its feasibility. The fourth part verifies the accuracy and feasibility of the method through five experiments. The fifth part summarizes the fault detection method of Deep EMD-PCA.

2. Fundamental Theory

2.1. EMD Method. EMD is a method to analyze the decomposition of nonlinear and nonstationary signals. It defines the time delay between the adjacent peak points of the signal to be decomposed as a time scale and decomposes the nonstationary signals into several Intrinsic Mode Function (IMF) and residual terms according to the fluctuation or trend of different scales [30]. Each basic pattern component reflects the local characteristic information of the signal. The remainder indicates the central trend of the signal. The flowchart of EMD signal decomposition is shown in Figure 1.

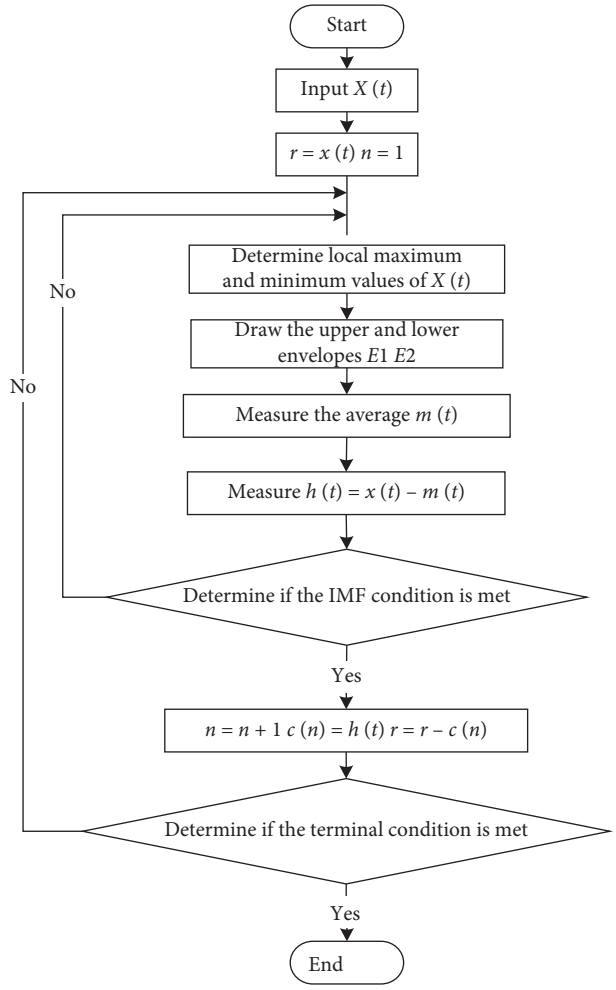

Figure 1: The structure of EMD.

For a group of signals $X(t)$, the steps of EMD are as follows.

Step 1. Find all maximum and minimum points of signal $X(t)$, respectively, and synthesize the upper and lower envelopes of the original data sequence by a cubic spline function.

Step 2. Calculate the mean value between upper and lower envelopes, denoted as $m_1(t)$. Subtract the mean value from the original data sequence to get a new data sequence h_1 with the low frequency being removed:

$$h_1 = X(t) - m_1(t). \tag{1}$$

If h_1 satisfies the following two conditions: (a) the number of crossing zero and extreme points must be equal or at most one difference in the whole dataset; (b) at any time, the average value of the local maximum and minimum envelopes should be zero, then, h_1 is the first IMF component.

If the conditions of IMF are not met, h_1 is taken as the original data, and the screening process (1) is repeated to obtain the difference h_{11} between the average value of the

upper and lower envelopes and h_1 and to determine whether the criteria of IMF are satisfied, until h_{1k} meets the above criteria of IMF, then h_{1k} is the first IMF component. Let us call the first IMF component IMF_1.

Step 3. Separate IMF_1 from $X(t)$ to obtain residual term r_1:

$$r_1 = X(t) - IMF_1, \tag{2}$$

r_1 is taken as the original data. Then, repeat steps (1) and (2) to obtain the second IMF component of $X(t)$–IMF_2. Repeat such screening process for n times to obtain n IMF components and residual term r_n of signal $X(t)$. When the residual term r_n is less than the preset value or becomes a monotone function, the components that meet the IMF conditions can no longer be extracted from it, and the whole screening process is finished.

After the above steps, signal $X(t)$ is decomposed into the sum of n IMF components and residual terms r_n:

$$X(t) = \sum_{i=1}^{n} \mathrm{IMF}_i(t) + r_n(t). \tag{3}$$

Theoretically, IMF components divide a series of locally high-order and low-order narrow-band stationary sequences strictly according to different characteristic scales of the sequence.

2.2. PCA Method. PCA method is a multivariate statistical method. It can achieve dimensionality reduction of complex samples; that is, it can generate reduced variables through feature extraction without losing important information carried in samples. Since the low-dimensional principal component space can retain most of the variance information of the original data space, and the orthogonality of the principal component variables can remove the redundant information of the original data space, principal component analysis has gradually become an effective method of data compression and information extraction. The basic theory of PCA is as follows.

Let the observation matrix $X \in R^{m\times n}$ be obtained through m times of independent sampling by n sensors. In order to eliminate the influence of false principal components caused by different dimensions, the sample $x_i(k)$ collected at the k moment should be standardized:

$$x_i^*(k) = \frac{x_i(k) - E(x_i)}{(\mathrm{var}(x_i))^{1/2}}, \tag{4}$$

where $i = 1, 2, \ldots, n$, $k = 1, 2, \ldots, m$. $E(x_i)$ is the sample mean and $\mathrm{var}(x_i)$ is the sample variance, as follows:

$$E\{x_i\} = \frac{1}{m}\sum_{k-1}^{m} x_i(k), \tag{5}$$

$$\mathrm{var}\{x_i\} = \frac{1}{m}\sum_{k-1}^{m} \left[x_i(k) - E\{x_i\}\right]^2. \tag{6}$$

The normalized sample matrix is $X^* \in R^{n*m}$:

$$X^* = \begin{pmatrix} x_1^*(1) & x_2^*(1) & \cdots & x_n^*(1) \\ \vdots & \vdots & \ddots & \vdots \\ x_1^*(m) & x_2^*(m) & \cdots & x_n^*(m) \end{pmatrix}. \tag{7}$$

The matrix X^* is decomposed into the cross product sum of n vectors:

$$X^* = t_1 p_1^T + t_2 p_2^T + \cdots + t_n p_n^T, \tag{8}$$

where $p_i \in R^n$ is the load vector; $P = [p_1, p_2, \ldots, p_n]$ is the load matrix. $t_i \in R^n$ is the goal vector and also is the principal component of X^*; $T = [t_1, t_2, \ldots, t_n]$ is the goal matrix and represents the projection of the original data matrix on the load direction.

The load vector of X^* can be obtained by Singular Value Decomposition (SVD), as follows:

$$\frac{1}{\sqrt{n-1}} X = U\Sigma V^T, \tag{9}$$

where $U \in R^{m\times n}$ and $V \in R^{n\times n}$ is the unitary matrix. $\Sigma \in R^{n\times n}$ is the diagonal matrix, and its diagonal elements are decreasing nonnegative eigenvalues.

Formula (12) is equal to the covariance matrix of X^*:

$$S = \frac{1}{n-1}(X^*)^T X^*. \tag{10}$$

Singular Value Decomposition is

$$S = P\Sigma P^T, \tag{11}$$

where the diagonal elements of $\Sigma \in R^{n\times n}$ are equal to the variance of X^* in the corresponding direction of the load matrix P. The projection of data X^* on the following load vector directions is often caused by noise, so in order to effectively remove the correlation of the original data and reduce the influence of interference, we retain the first load vector corresponding to the first maximum eigenvalue to compose the load matrix $P \in R^{n\times a}$.

The original space is divided into principal component subspace $\hat{X}$ and residual subspace E:

$$X^* = \hat{X} + E = TP^T + E. \tag{12}$$

As for the selection method of principal components, we adopted the Cumulative Percentage Variance (CPV) method:

$$\mathrm{CPV} = \left[\frac{\sum_{i=1}^{t}\lambda_i}{\sum_{i=1}^{n}\lambda_i}\right] \times 100\%, \tag{13}$$

where n is the number of variables in the data and λ_i is the i^{th} eigenvalue of the covariance matrix of X. The threshold percentage is usually set at 85%.

3. Deep EMD-PCA

The commonly used EMD-PCA combined fault detection method can analyze the vibration signal for fault detection. However, due to the limitations of the PCA method, some fault features are discarded during the process of extracting

the principal elements, which may result in PCA not being able to accurately detect weak incipient failure message. Therefore, this paper proposes a fault detection method based on Deep EMD-PCA.

3.1. The Fundamental Deep EMD-PCA. Firstly, the EMD method is used to decompose the vibration signal to obtain n IMF components, then the n IMF components are formed into a matrix, and the eigenvalue decomposition of the matrix is obtained by the PCA method to obtain the principal element space and the residual space. Then, the principal space and the residual space are decomposed multiple times to obtain the j-layer subspace, the statistics and control limits of each subspace are calculated, and a comparison is made to determine whether a fault has occurred. The data structure of Deep EMD-PCA is shown in Figure 2.

We obtain the principal element space and the residual space of dataset IMF by EMD-PCA method:

$$\mathrm{IMF} = \mathrm{IMF}_{11} + \mathrm{IMF}_{12}, \tag{14}$$

where IMF_{11} is the first-order principal component subspace of original data IMF and IMF_{12} is the first-order residual subspace of original data IMF. They can be obtained by

$$\begin{aligned} \mathrm{IMF}_{11} &= P_{11}P_{11}^{T}\mathrm{IMF}, \\ \mathrm{IMF}_{12} &= \left(I - P_{11}P_{11}^{T}\right)\mathrm{IMF}, \end{aligned} \tag{15}$$

Where P_{11} is the is the extracted principal component feature vector matrix of IMF.

To obtain more information about the second-order principal component space and residual space, we repeat the above process and then obtain

$$\begin{aligned} \mathrm{IMF}_{11} &= \mathrm{IMF}_{21} + \mathrm{IMF}_{22}, \\ \mathrm{IMF}_{12} &= \mathrm{IMF}F_{23} + \mathrm{IMF}_{24}. \end{aligned} \tag{16}$$

Suppose that P_{21} and P_{23} are the principal vector of IMF_{11} and IMF_{12}, respectively, and P_{22} and P_{24} are the residual vector of IMF_{11} and IMF_{12}, respectively. Then, the original data IMF can be obtained by

$$\begin{aligned} \mathrm{IMF} &= \mathrm{IMF}_{11} + \mathrm{IMF}_{12}, \\ &= \mathrm{IMF}_{21} + \mathrm{IMF}_{22} + \mathrm{IMF}_{23} + \mathrm{IMF}_{24}, \end{aligned} \tag{17}$$

where

$$\begin{aligned} \mathrm{IMF}_{21} &= P_{21}P_{21}^{T}\mathrm{IMF}_{11}, \\ \mathrm{IMF}_{22} &= \left(I - P_{21}P_{21}^{T}\right)\mathrm{IMF}_{11}, \\ \mathrm{IMF}_{23} &= P_{23}P_{23}^{T}\mathrm{IMF}_{12}, \\ \mathrm{IMF}_{24} &= \left(I - P_{23}P_{23}^{T}\right)\mathrm{IMF}_{12}. \end{aligned} \tag{18}$$

By parity of reasoning, the original data IMF can be represented as the sum of 2^j subspace, and j is the order. The structure of Deep EMD-PCA is shown in Figure 2. The subspace IMF_{jk} can be expressed as

$$\mathrm{IMF}_{jk} = \begin{cases} P_{jk}P_{jk}^{T}\mathrm{IMF}_{(j-1)(k+1)/2}, & k \text{ is odd}, \\ \left(I - P_{j(k-1)}P_{j(k-1)}^{T}\right)\mathrm{IMF}_{(j-1)(k/2)}, & k \text{ is even}. \end{cases} \tag{19}$$

Suppose that IMF_{jk} is the k^{th} subspace of j^{th} order; then, $\mathrm{IMF} = \sum_{k=1}^{2^j}\mathrm{IMF}_{jk}$, and P_{jk} is the extracted principal component feature vector matrix of $\mathrm{IMF}_{(j-1(k+1)/2)}$.

Through the increase in the order of the Deep EMD-PCA method, extremely weak fault information can be detected, thereby achieving incipient fault detection.

3.2. Determination of Statistics and Control Limits. We extend the method of statistical control limit to Deep EMD-PCA. Considering all subprincipal spaces, $T^2{}_{jk}$ of each subdataset X_{jk} can be expressed as

$$T_{jk}^{2} = \mathrm{IMF}^{T}P_{(j+1)(2k-1)}\Lambda_{jk}^{-1}P_{(j+1)(2k-1)}^{T}\mathrm{IMF}. \tag{20}$$

Λ_{jk} is principal component space characteristic value of matrix.

For the control limit of $T^2{}_{jk}$, it can be calculated through the preset significance level α and the probability density function of $T^2{}_{jk}$. The probability density function of $T^2{}_{jk}$ can be expressed as

$$f\left(T_{jk}^{2}\right) = \frac{1}{N}\sum_{b=1}^{N}K\left(\frac{1}{h}\left(T_{jk}^{2} - T_{jk}^{b}\right)\right), \tag{21}$$

where T_{jk}^{b} represents T_{jk}^{2} of column b. Then, the probability density function is integrated to make it less than the significance level alpha, namely,

$$\int_{0}^{\mathrm{TUCL}_{jk}} f\left(T_{jk}^{2}\right)dT_{jk}^{2} = \alpha. \tag{22}$$

SPE statistics reflect the deviation degree of data, which can be expressed as

$$\mathrm{SPE}_{jk} = \left\|\left(I - P_{(j+1)(2k-1)}P_{(j+1)(2k-1)}^{T}\right)\mathrm{IMF}^{2}\right\|. \tag{23}$$

Similar to the control limit of T_{jk}^{b}, the probability density function of SPE_{jk} is expressed as

$$f\left(\mathrm{SPE}_{jk}\right) = \frac{1}{N}\sum_{b=1}^{N}K\left(\frac{1}{h}\left(\mathrm{SPE}_{jk} - \mathrm{SPE}_{jk}^{b}\right)\right), \tag{24}$$

where SPE_{jk}^{b} represents SPE_{jk} of column b, according to the probability density function and significance level a, namely,

$$\int_{0}^{\mathrm{QUCL}_{jk}} f\left(\mathrm{SPE}_{jk}\right)d\mathrm{SPE}_{jk} = \alpha. \tag{25}$$

If the statistics is larger than the control limit, a fault will occur. Otherwise, the data are in a normal state.

3.3. Theoretical Proof. This section demonstrates the incipient fault detection capabilities of Deep EMD-PCA from a theoretical perspective.

The covariance of Deep EMD-PCA can be expressed as

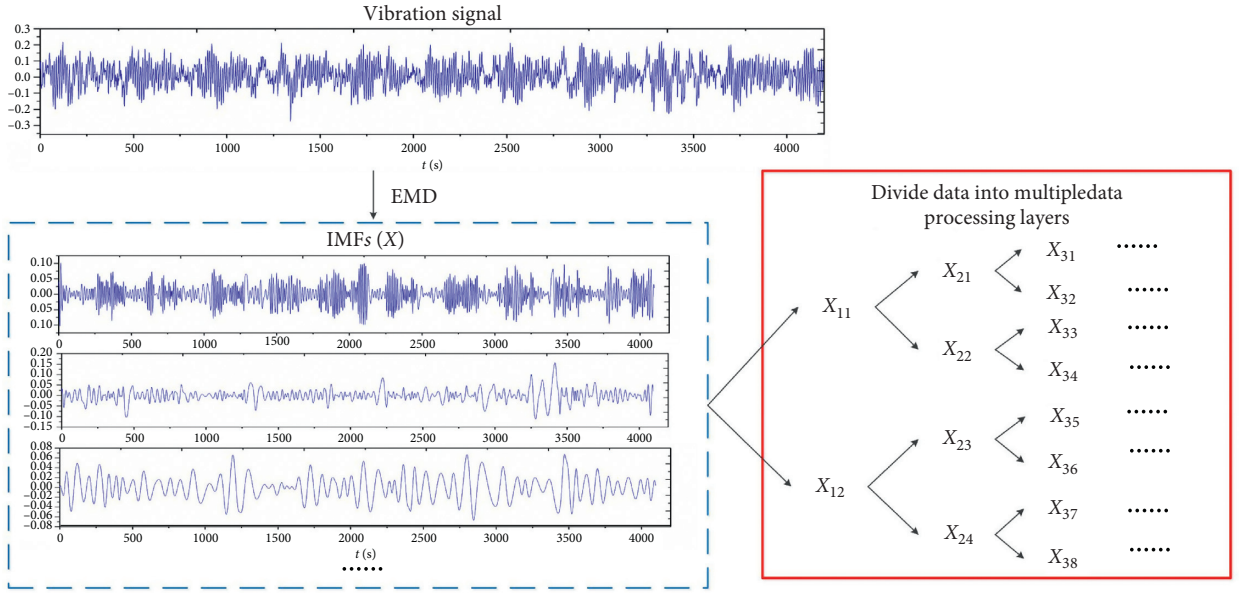

Figure 2: The data structure of Deep EMD-PCA.

$$S = \frac{1}{N-1}\mathrm{IMF}^T\mathrm{IMF}. \tag{26}$$

The size of the covariance represents the amount of information retained by the method, so the larger the covariance, the more information retained.

According to formula (14), we can obtain that

$$S = \frac{1}{N-1}\left(\mathrm{IMF}_{11} + \mathrm{IMF}_{22}\right)^T\left(\mathrm{IMF}_{11} + \mathrm{IMF}_{22}\right). \tag{27}$$

For the j^{th} subspace, the covariance can be expressed as

$$S = \frac{1}{N-1}\left(\sum_{k=1}^{2^j}\mathrm{IMF}_{jk}\right)^T\left(\sum_{k=1}^{2^j}\mathrm{IMF}_{jk}\right). \tag{28}$$

We simplify formula (28):

$$\begin{aligned} S &= \frac{1}{N-1}\sum_{k=1}^{2^j}\left\{\left(\mathrm{IMF}_{jk}\right)^T\left(\mathrm{IMF}_{jk}\right)\right\}, \\ &= \sum_{k=1}^{2^j}\frac{1}{N-1}\left\{\left(\mathrm{IMF}_{jk}\right)^T\left(\mathrm{IMF}_{jk}\right)\right\}. \end{aligned} \tag{29}$$

Suppose that $S_{jk} = (1/(N-1))\mathrm{IMF}_{jk}^T\mathrm{IMF}_{jk}$; then, the covariance matrix can be simplified as

$$\begin{aligned} S &= S_{11} + S_{12}, \\ &= \sum_{k=1}^{3} S_{2k} + S_{24} = \ldots, \\ &= \sum_{k=1}^{2^j-1} S_{jk} + S_{j2^j}. \end{aligned} \tag{30}$$

So, we can obtain that $\sum_{k=1}^{2^j-1} S_{jk} > \ldots > \sum_{k=1}^{3} S_{2k} > S_{11}$. Because the covariance matrix describes all the information about the relationships among the dimensions, it can be concluded that as the order increases, the information retained by Deep EMD-PCA increases. Therefore, the Deep EMD-PCA method can retain more sample information compared with the traditional EMD-PCA method, so as to mine the hidden fault information in the sample abandoned by EMD-PCA to achieve the purpose of incipient fault detection.

We can project the dataset IMF in normal operation into the third-order principal space and the residual space based on equations (14)–(18), as shown in Figure 3. For the conventional EMD-PCA method, the residual is IMF_{12}. The residual of the second order of the Deep EMD-PCA method is IMF_{24}. The residual of the third order of the Deep EMD-PCA method is IMF_{38}. According to Figure 3, it can be seen that the residual amount IMF_{12} is significantly larger than IMF_{24}, and IMF_{24} is larger than IMF_{38}. Therefore, we can conclude that with the increase of the order, the residual of the Deep EMD-PCA method is getting smaller and smaller, that is, the more variance information saved, so that the weak fault information can be diagnosed.

However, with the increase in order, the amount of calculation increases gradually. Considering the complexity of the calculation, it is usually calculated to the third order to mine the weak fault information in the dataset.

As can be seen from Figure 3, all subspaces and subdatasets are orthogonal. So, the 2^j subdatasets of original data are nonoverlapping, there is no duplicate information, and it can contain all information on the dataset.

3.4. The Process of Deep EMD-PCA. The fault detection method based on Deep EMD-PCA is divided into two parts: offline modeling and online monitoring. The Deep EMD-PCA approach is defined by Algorithm 1.

4. Experimental Results and Analysis

This section uses the experimental data of Case Western Reserve University and the self-built mechanical failure

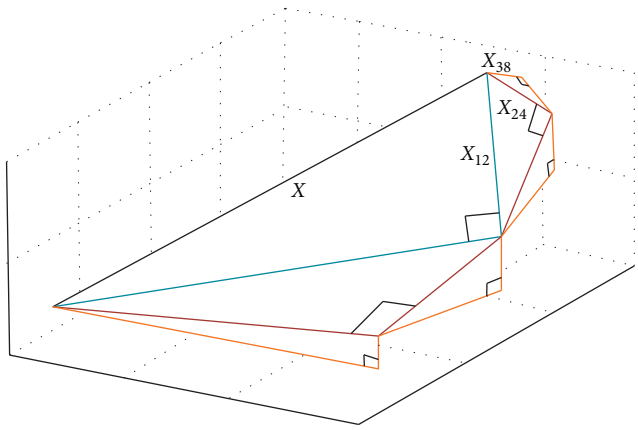

Figure 3: The geometry structure of Deep EMD-PCA.

comprehensive simulation testbed to collect the failure vibration data of the inner and outer rings of the rolling bearing. The PCA-SVM fault diagnosis method first reduces the dimensionality of the data through PCA and then puts the later data into the SVM model for classification. This method has advantages in processing small samples and is not sensitive to noise data and feature vectors. For many scenarios, the model can be built quickly, and good results can usually be achieved. Comparing the EMD-PCA method and PCA-SVM method with the Deep EMD-PCA method proposed in this paper, it proves the feasibility of the early fault detection method proposed in this paper.

The failure types are the inner ring failure and the outer ring failure of the rolling bearing. The failure mechanism of the inner and outer ring failure of the rolling bearing is analyzed, and the results are as follows:

(1) The inner ring failure: since the inner ring rotates with the rolling bearing during the operation of the rolling bearing, when a certain failure occurs in the inner ring of the rolling bearing, the failure point and the magnitude of the pulse intensity have a certain consistency, and the amplitude will also show periodic changes. In the process of collecting vibration signals, the signal reflecting the fault information of the inner ring will be affected by the impact vibration, resulting in the loss of high-frequency vibration components, resulting in a certain energy loss, so the detection of the inner ring fault of the rolling bearing is more difficult

(2) The outer ring failure: due to a certain failure in the outer ring of the rolling bearing, the vibration signal will show a periodic pulse force whenever the operation passes the failure point. Different from the inner ring failure, since the outer ring is generally fixed, the pulse intensity of each cycle is constant. Therefore, the detection of the outer ring failure is relatively simple compared to the detection of the inner ring failure of the rolling bearing

4.1. The Experimental Data of Case Western Reserve University. In this section, the experimental data of Case Western Reserve University is used to verify the Deep EMD-PCA method. In this experiment, three groups of experimental data were collected, namely, vibration signal data under normal condition, fault data of bearing inner ring with fault diameter of 0.007 inches, and fault data of bearing outer ring with fault diameter of 0.007 inches. The fault diameter is 0.007 inches, which is very small. At this time, the fault characteristics are relatively weak. Therefore, this fault is considered to be an incipient fault. The vibration acceleration signal of the bearing is collected by the acceleration sensor, and the motor speed is 1797 RPM.

Figures 4(a) and 4(b) illustrate the T^2 and SPE fault detection results based on the EMD-PCA fault detection method for an outer ring fault with a fault diameter of 0.007 inches. The abscissa is the number of samples, and the ordinate is the statistics and the control limit. Among them, the blue line indicates the statistics, and the red line indicates the control limit. When the statistics exceeds the control limit, it indicates that the data is detected as faulty. From Figures 4(a) and 4(b), we obtain that T_{01}^2 and SPE_{01} are less affected by this fault.

Figure 5 shows the results of the PCA-SVM method of detecting the failure of the inner ring of the rolling bearing. Label 0 means normal data, and label 1 means inner ring fault data. The blue circle represents the predicted result, and the red cross represents the actual diagnosis result. We can see from the image that the detection rate is about 60%, and the incipient fault detection results are not satisfactory.

Figures 6 illustrates the T^2 and SPE fault detection results based on the Deep EMD-PCA fault detection method for an outer ring fault with a fault diameter of 0.007 inches. Figures 6(a)–6(d) describe the result of the second-layer datasets IMF_{11} and IMF_{12}. Figures 6(e)–6(l) describe the third-layer datasets IMF_{21}–IMF_{24}. In Figure 6(d), the impact of SPE_{12} by this fault is more obvious, and other statistics are less affected by this fault. In Figure 6(k), the influence of T_{24}^2 is very large, and the rate of detection is about 85%. Therefore, the fault detection of the third layer of Deep EMD-PCA is better.

Figure 7 depicts the results of a fault detection based on the EMD-PCA fault detection method for an outer ring fault with a fault diameter of 0.007 inches. From Figures 7(a) and 7(b), we can obtain that the detection rate of the fault detection result of the first layer of Deep EMD-PCA exceeds 50%.

Figure 8 shows the results of the PCA-SVM method of detecting the failure of the inner ring. Label 0 means normal data, and label 1 means inner ring fault data. The blue circle represents the predicted result, and the red cross represents the actual diagnosis result. We can see from the image that the detection rate is about 45%, and the incipient fault detection results are not satisfactory.

Figure 9 depicts the results of a fault detection based on the Deep EMD-PCA fault detection method for an outer ring fault with a fault diameter of 0.007 inches. Figures 9(a)–9(d) describe the result of the second-layer datasets IMF_{11} and IMF_{12}. Figures 9(e)–9(l) describe the third-layer datasets IMF_{21}–IMF_{24}. In Figure 9(d), the result of SPE_{12} is greatly affected by the fault of the third layer of Deep EMD-PCA.

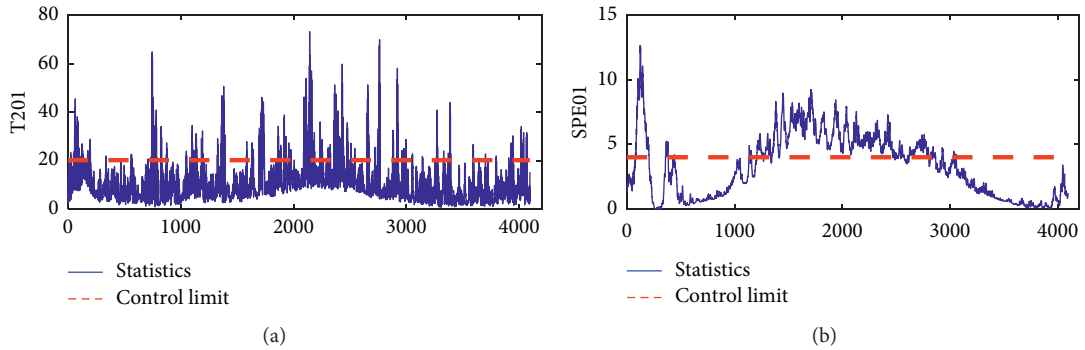

Figure 4: Case Western Reserve University bearing inner ring failure results based on EMD-PCA.

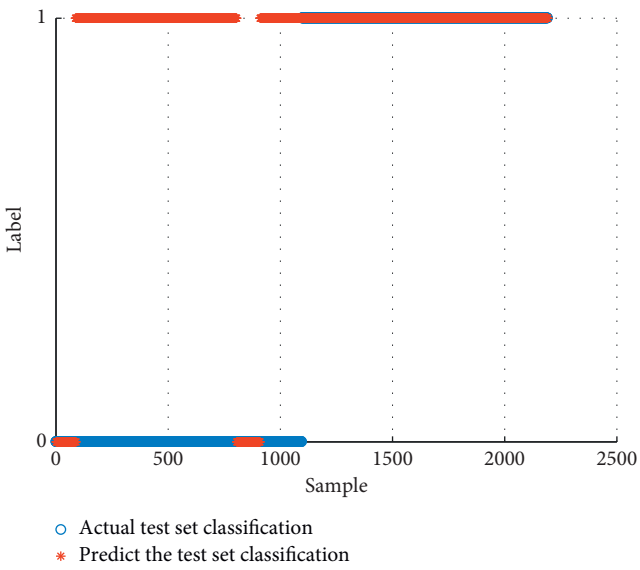

Figure 5: Case Western Reserve University bearing inner ring failure results based on PCA-SVM.

The detection results show that T_{24}^2 is most affected by this fault, and the detection rate is about 85%. Therefore, the third layer of Deep EMD-PCA has good fault detection performance.

We compare the experimental results of the Deep EMD-PCA proposed in this paper, EMD-PCA method, and PCA-SVM method by analyzing the detection rate and detection delay as shown in Table 1.

The detection rate refers to the percentage of the number of accurate sampling points in the detection process to the total number of sampling points. The detection delay time refers to the interval from the start of the failure to the detection of the failure. Table 1 describes the comparison results of the detection rate and detection delay based on the EMD-PCA, PCA-SVM, and Deep EMD-PCA methods. From Table 1, for the inner ring fault, the detection rate of EMD-PCA method and PCA-SVM method is 49.44% and 58.71%, respectively, and the detection rate of Deep EMD-PCA method is 86.92%; for outer ring fault, the detection rate of EMD-PCA and PCA-SVM is about 50%, and the detection rate of Deep EMD-PCA method is 86.77%, so we can obtain that the detection rate of Deep EMD-PCA method is significantly increased. On the other hand, from the comparison of detection delay, Deep EMD-PCA can be detected from the beginning of the fault. So, the Deep EMD-PCA method has good fault detection performance.

4.2. Mechanical Failure Comprehensive Simulation Experiment. The mechanical failure comprehensive simulation experimental device includes a mechanical fault comprehensive simulation test bench, AIC9916FS equipment fault comprehensive simulation diagnostic analysis system software, FL6816L16 channel sensor, BSZ800D-16 vibration signal acquisition instrument, and storage device computer. The mechanical failure comprehensive simulation test bench is shown in Figure 10. Through this test bench, the fault data of the outer ring, inner ring, and rolling element of the bearing are collected and analyzed.

Figure 11 depicts the results of a fault detection based on the EMD-PCA fault detection method for an outer ring fault. From Figures 9(a) and 9(b), we can obtain that the false detection rate of the detection result of the first layer of Deep EMD-PCA is more than 80%.

Figure 12 depicts the mechanical failure comprehensive simulation experiment bearing outer ring failure results based on PCA-SVM. Label 0 means normal data, and label 1 means outer ring fault data. The blue circle represents the predicted result, and the red cross represents the actual diagnosis result. We can see from the image that the detection rate is about 80%, and the incipient fault detection results are not satisfactory.

Figure 13 depicts the results of a fault detection based on the Deep EMD-PCA fault detection method for an outer ring fault. Figures 13(a)–13(d) describe the result of the second-layer datasets dataset IMF_{11} and IMF_{12}. Figures 13(e)–13(l) describe the third-layer datasets IMF_{21}–IMF_{24}. In Figure 13(b), the result of SPE_{11} is greatly affected by this fault. In Figures 13(e) and 13(j)–13(l), T_{21}^2, SPE_{23}, T_{24}^2, and SPE_{24} are more affected by this fault. Therefore, the fault detection effect of the third-layer Deep EMD-PCA is better, which proves that the method has better incipient fault detection capability.

Figure 14 depicts the results of a fault detection based on the Deep EMD-PCA fault detection method for an inner

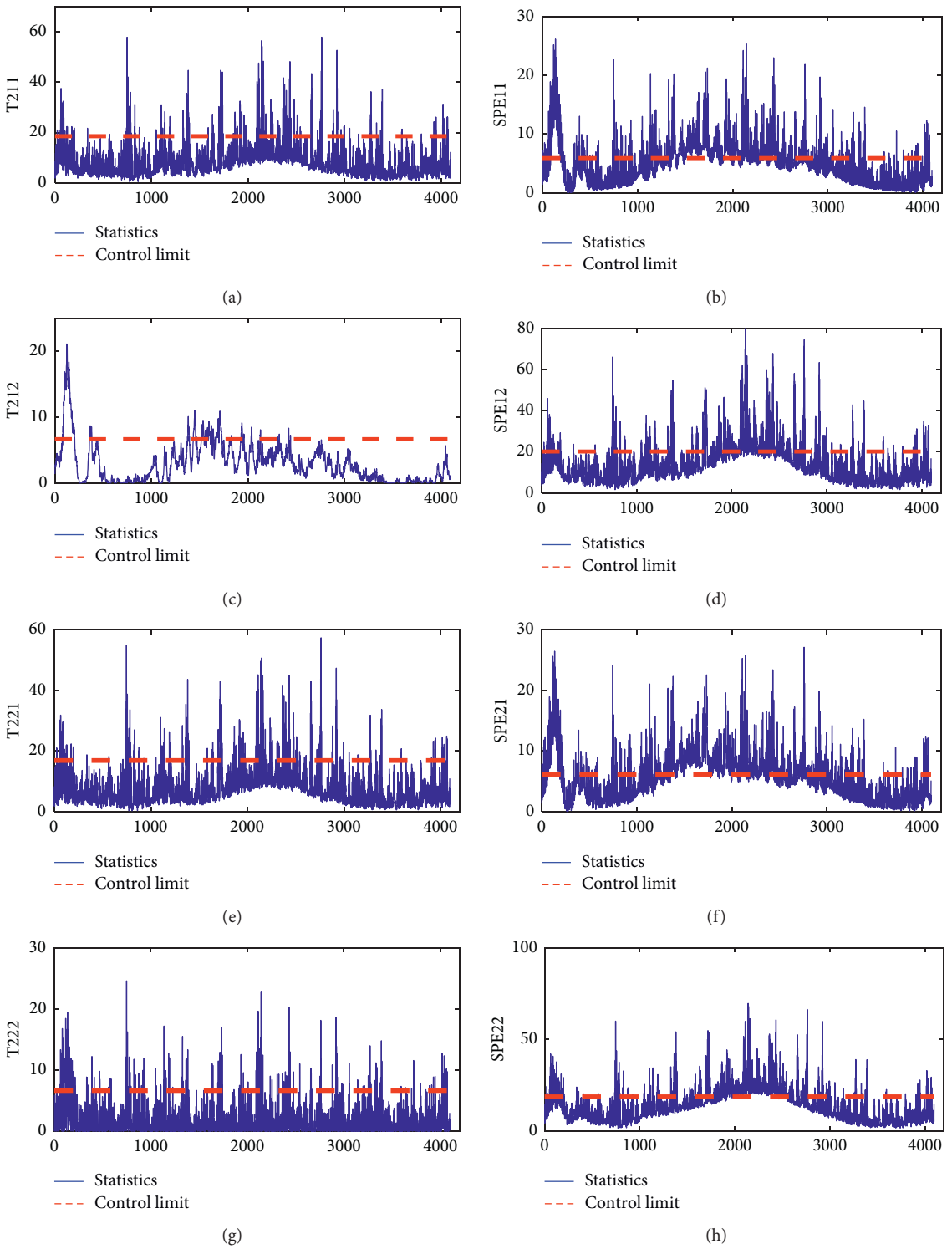

Figure 6: Continued.

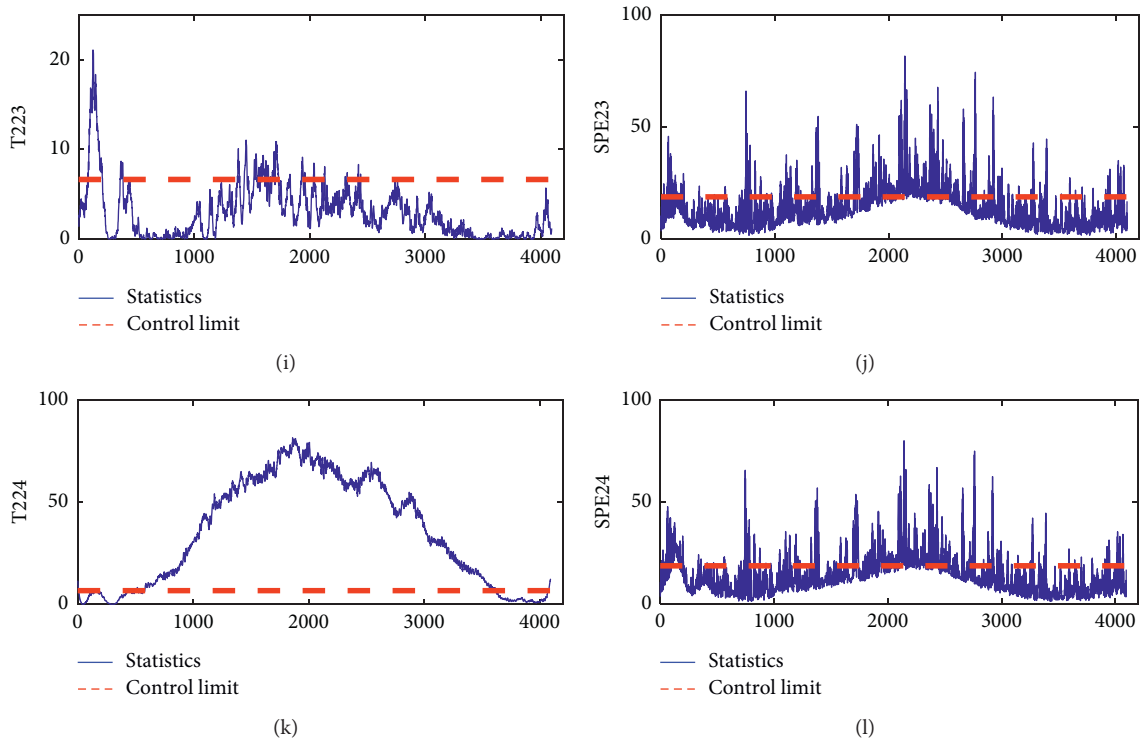

Figure 6: Case Western Reserve University bearing inner ring failure results based on Deep EMD-PCA.

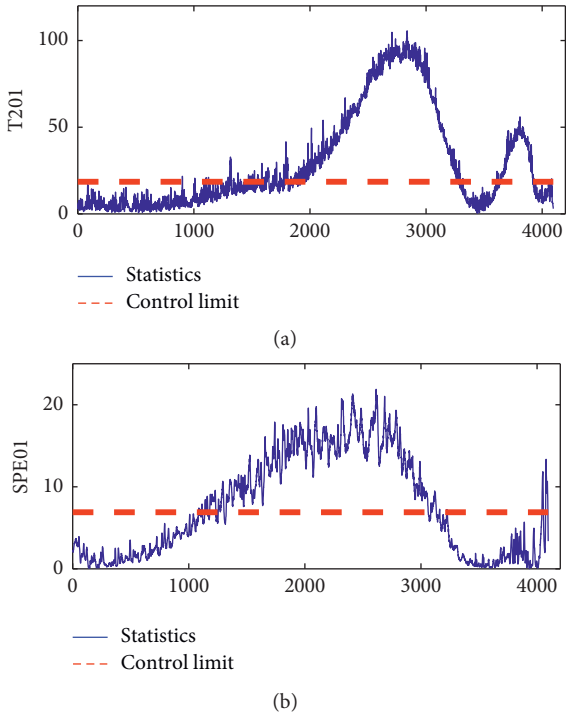

Figure 7: Case Western Reserve University bearing outer ring failure results based on EMD-PCA.

ring fault. From Figures 14(a) and 14(b), we can obtain that the detection rate of the fault detection result of the first layer of Deep EMD-PCA is more than 60%.

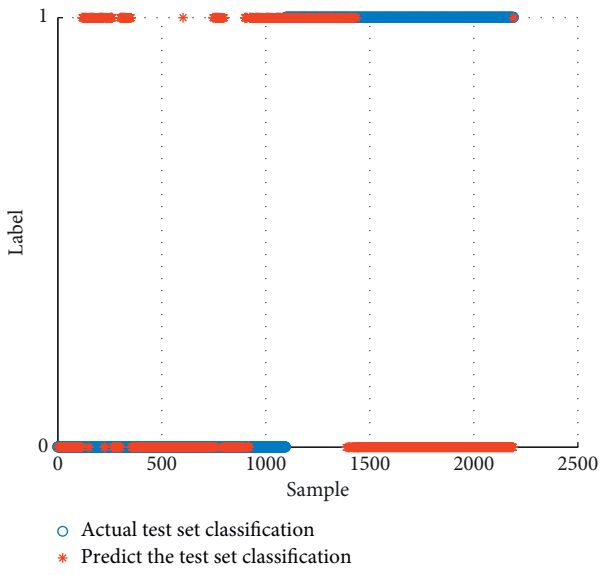

Figure 8: Case Western Reserve University bearing outer ring failure results based on PCA-SVM.

Figure 15 depicts the mechanical failure comprehensive simulation experiment bearing inner ring failure results based on PCA-SVM. Label 0 means normal data, and label 1 means inner ring fault data. The blue circle represents the predicted result, and the red cross represents the actual diagnosis result. We can see from the image that the detection rate is about 85%.

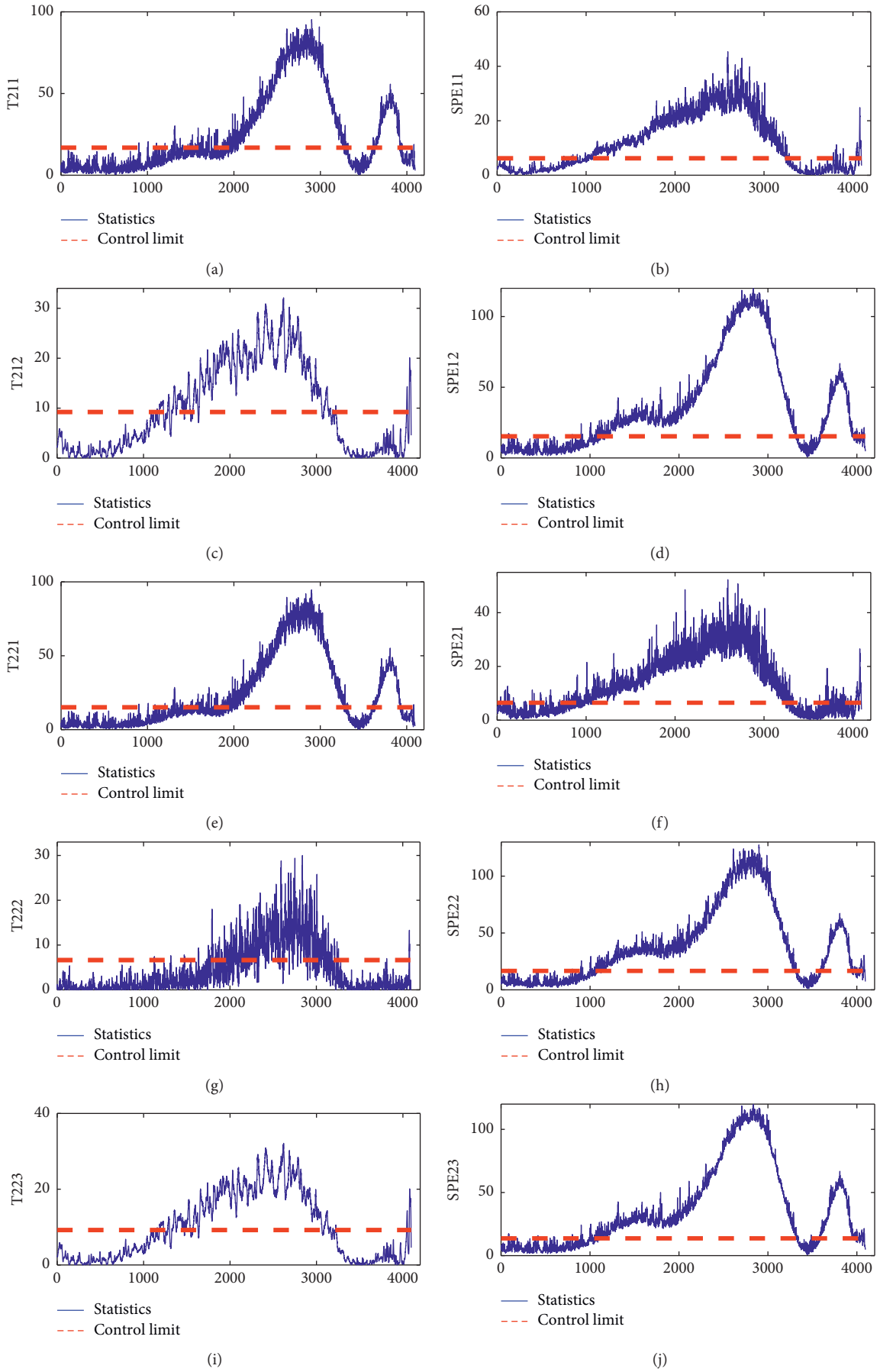

Figure 9: Continued.

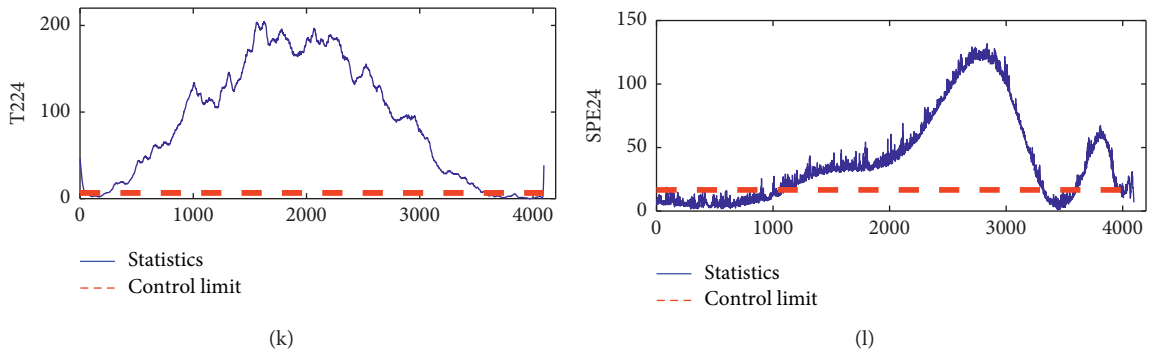

(k) (l)

Figure 9: Case Western Reserve University bearing outer ring failure results based on Deep EMD-PCA.

(1) Offline modeling:
(2) $X(t)$ is the training dataset
(3) Perform EMD decomposition to obtain n IMF components and residual Rn
(4) Group n IMF components into a new matrix IMF
(5) Standardization processing for IMF
(6) Select the appropriate order j
(7) Calculate the corresponding IMF_{jk}
(8) Calculate the number of principals of each IMF_{jk}, the eigenvalue matrix Λ_{jk}, and the eigenvector matrix P_{jk}
(9) Calculate the statistics T^2_{jk} and SPE_{jk}
(10) Calculate the probability density function of T^2_{jk} and SPE_{jk}
(11) Calculate the control limits of T^2_{jk} and SPE_{jk}
(12) Online Monitoring:
(13) $Xt(t)$ is the test dataset
(14) Perform EMD decomposition to obtain n IMF components and residual Rn
(15) Group n IMF components into a new matrix IMFt
(16) Standardization processing for IMFt
(17) Obtain the principal element space and the residual space of the subdataset $\mathrm{IMF}t_{jk}$
(18) Calculate the statistics T^2_{jk} and SPE_{jk}
(19) If the statistics > the control limits
(20) Then fault
(21) Else normal
(22) End if

Algorithm 1:Deep EMD-PCA.

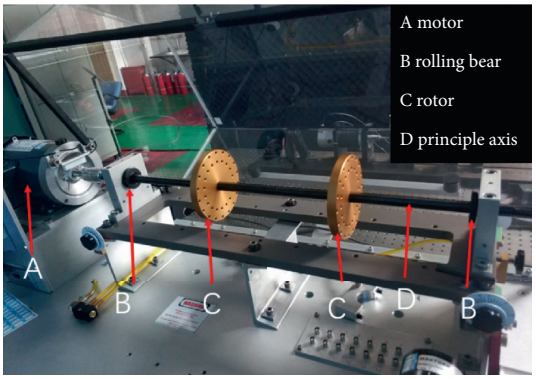

Figure 10: Mechanical fault comprehensive simulation test bench.

Figures 16(a)–16(d) describe the result of the second-layer datasets dataset IMF_{11} and IMF_{11}. Figures 16(e)–16(l) describe the third-layer datasets IMF_{21}–IMF_{24}. In Figures 16(b) and 16(d), the results of SPE_{11} and SPE_{12} are greatly affected by this fault. In Figures 16(h) and 16(j)–16(l), SPE_{22}, SPE_{23}, T^2_{24}, and SPE_{24} are more affected by this fault.

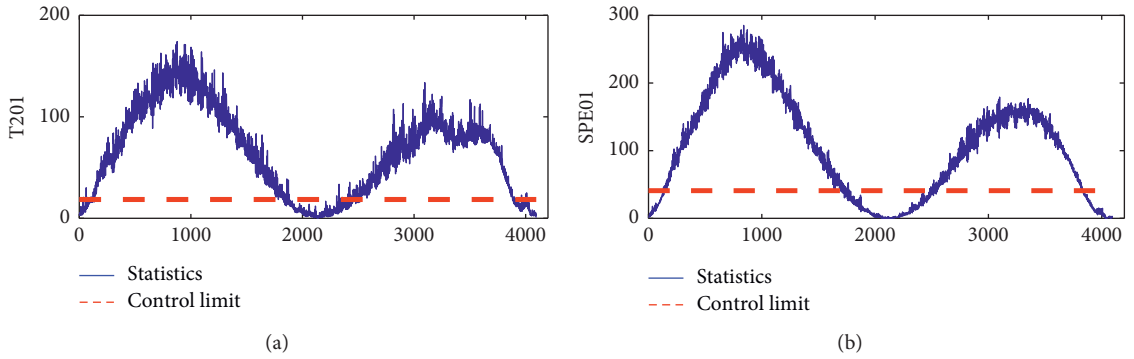

Figure 11: Mechanical failure comprehensive simulation experiment bearing outer ring failure results based on EMD-PCA.

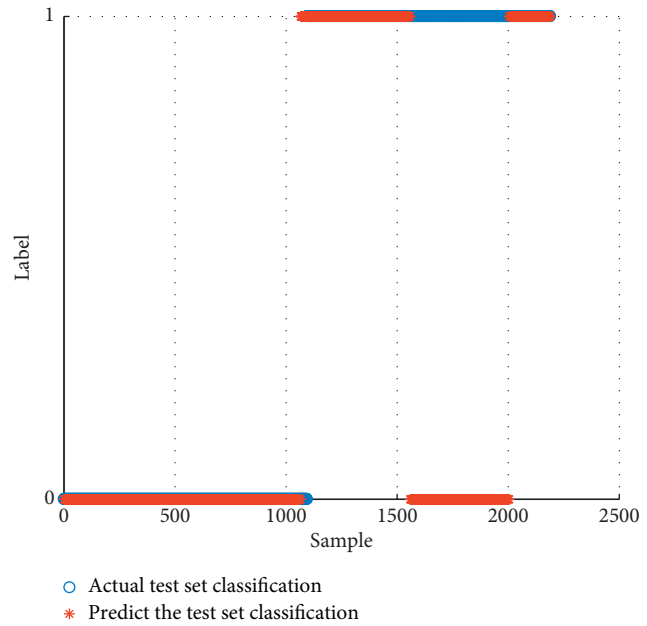

Figure 12: Mechanical failure comprehensive simulation experiment bearing outer ring failure results based on PCA-SVM.

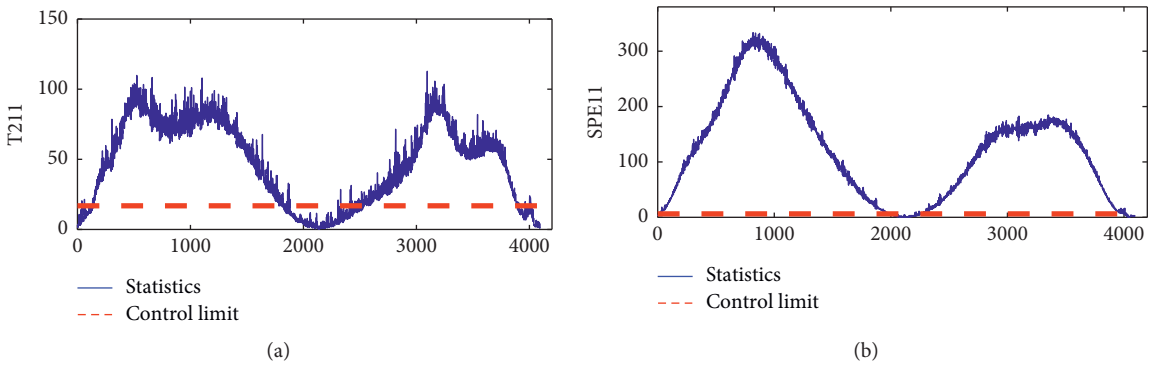

Figure 13: Continued.

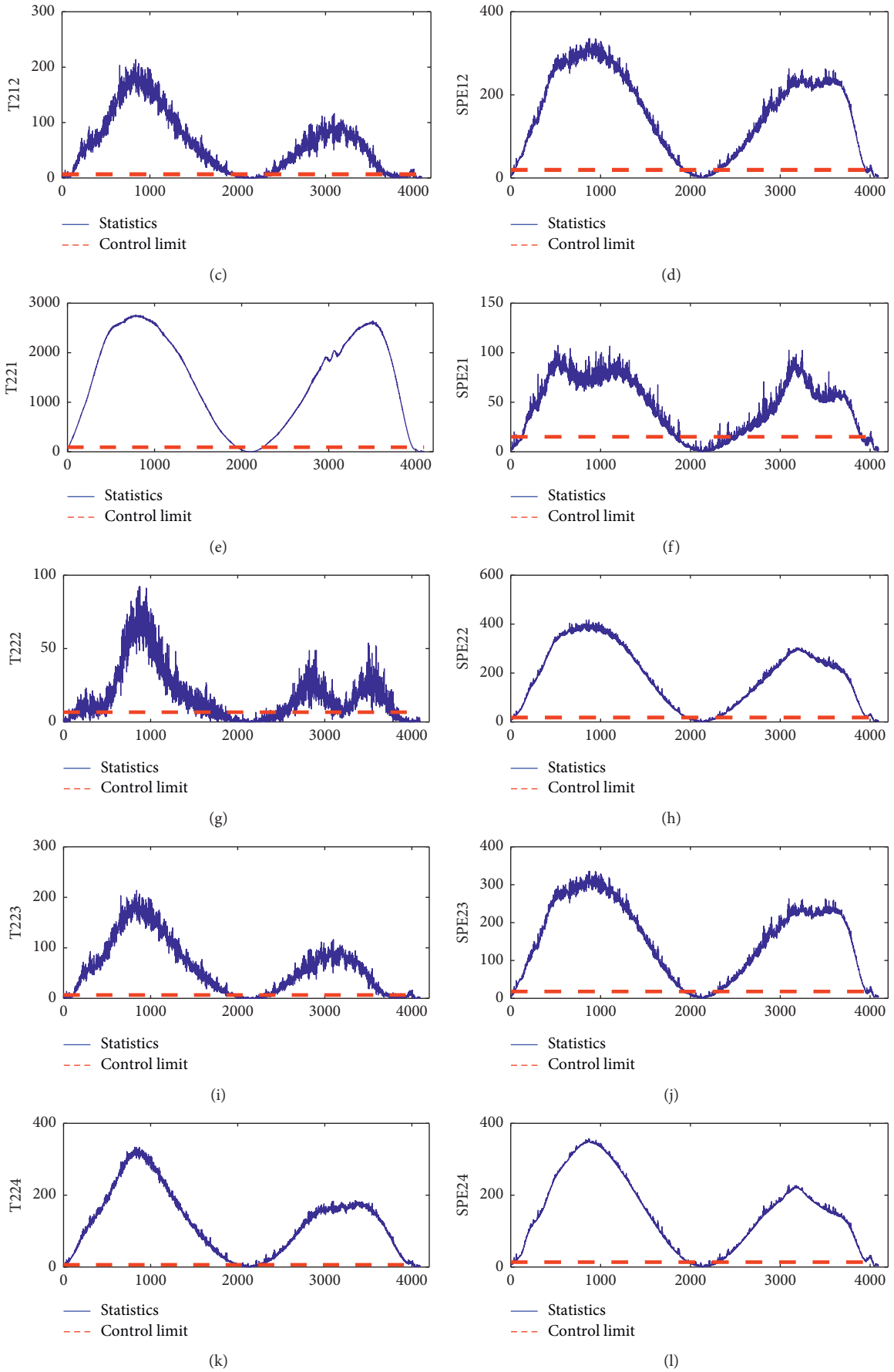

Figure 13: Mechanical failure comprehensive simulation experiment bearing outer ring failure results based on Deep EMD-PCA.

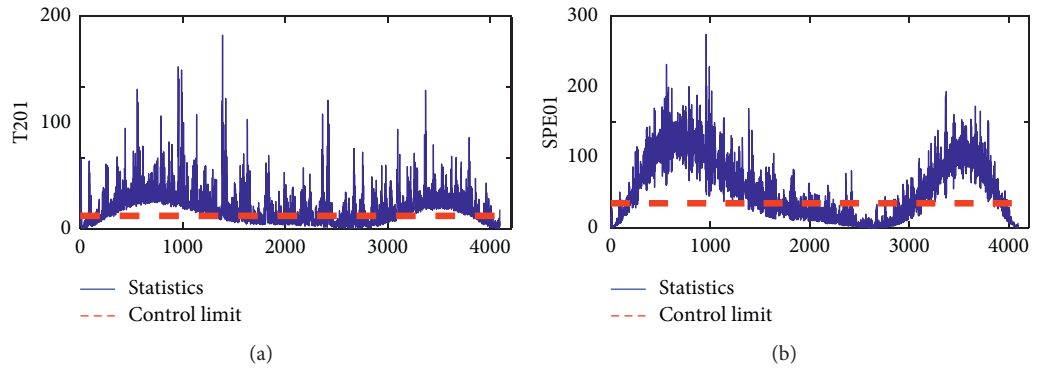

Figure 14: Mechanical failure comprehensive simulation experiment bearing inner ring failure results based on EMD-PCA.

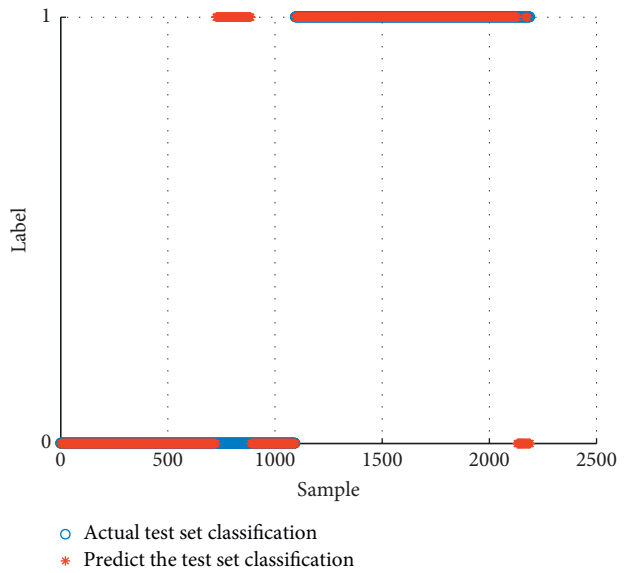

Figure 15: Mechanical failure comprehensive simulation experiment bearing inner ring failure results based on PCA-SVM.

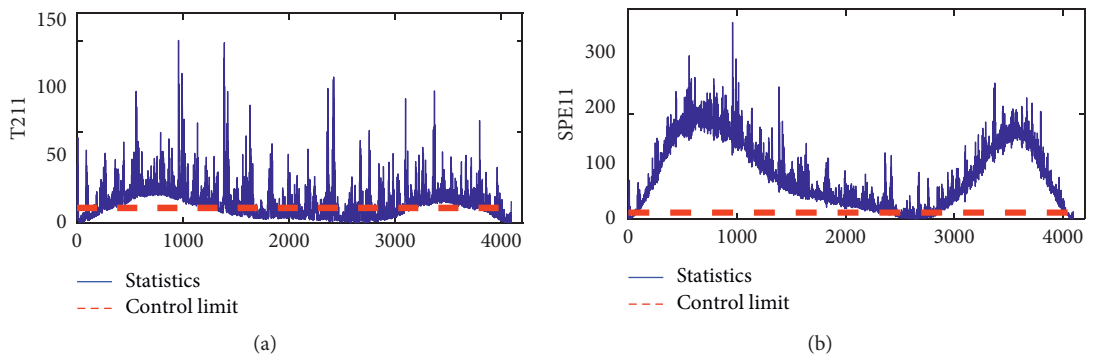

Figure 16: Continued.

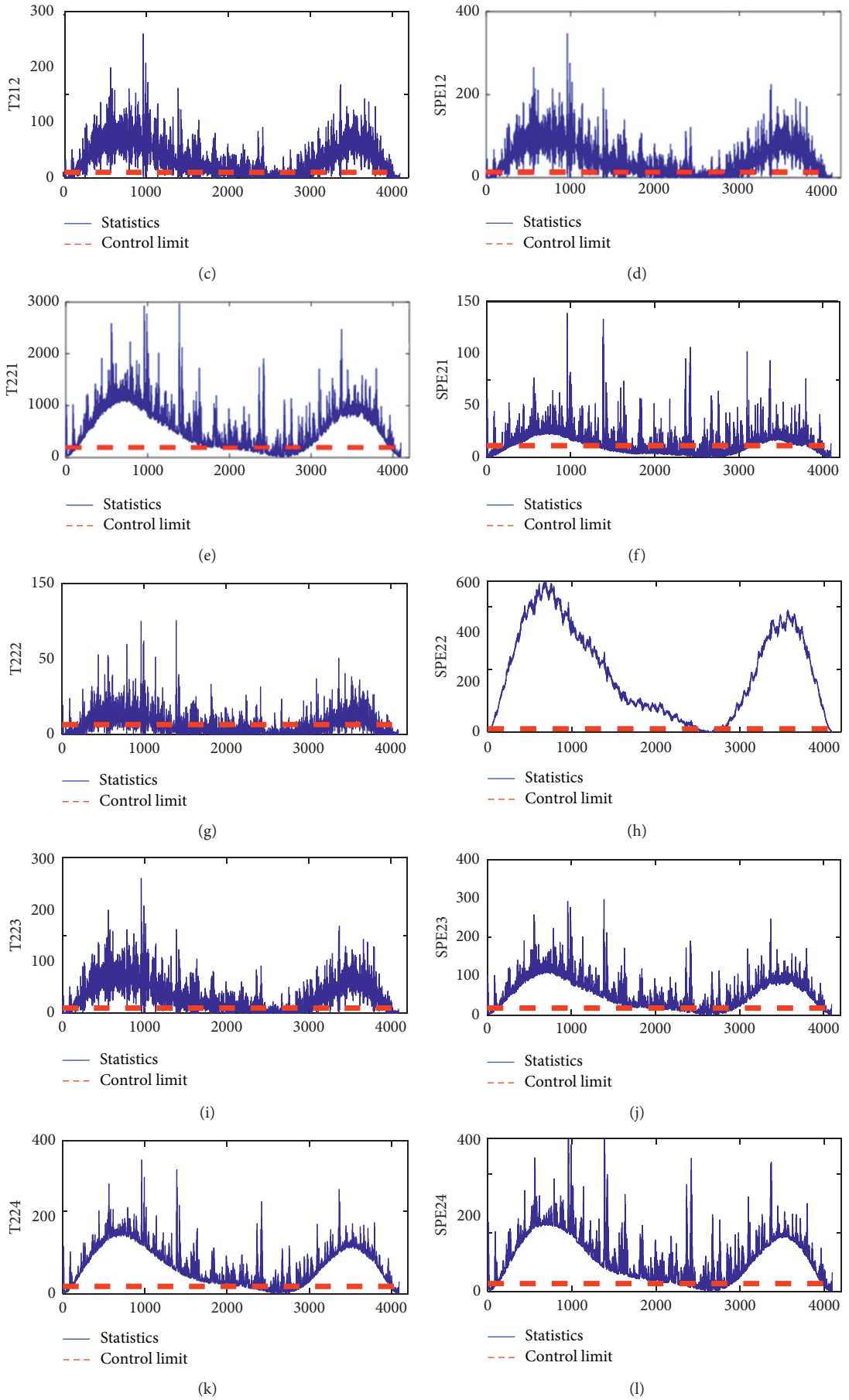

Figure 16: Mechanical failure comprehensive simulation experiment bearing inner ring failure results based on Deep EMD-PCA.

Table 1: Experimental performance comparison of Case Western Reserve University.

Fault	EMD-PCA		PCA-SVM	Deep EMD-PCA	
	Detection rate (%)	Detection delay	Detection rate (%)	Detection rate (%)	Detection delay
Inner ring fault	49.44	74	58.71	86.92	0
Outer ring fault	47.98	901	45.44	86.77	0

Table 2: Experimental performance comparison of mechanical failure comprehensive.

Fault	EMD-PCA		PCA-SVM	Deep EMD-PCA	
	Detection rate (%)	Detection delay	Detection rate (%)	Detection rate (%)	Detection delay
Outer ring fault	74.94	115	78.26	90.87	15
Inner ring fault	54.29	11	86.72	91.36	3

Therefore, the fault detection effect of the third-layer Deep EMD-PCA is better, which proves that the method has better incipient fault detection capability.

We compare the experimental results of the Deep EMD-PCA proposed in this paper, the traditional EMD-PCA method, and the PCA-SVM method by analyzing the detection rate and detection delay as shown in Table 2.

Table 2 describes the comparison results of the detection rate and detection delay based on the EMD-PCA, PCA-SVM, and Deep EMD-PCA methods. For the outer ring fault, the detection rate of EMD-PCA method and PCA-SVM method is about 75%, and the detection rate of the Deep EMD-PCA method is 90.87%; for outer ring fault, the detection rate of EMD-PCA and PCA-SVM is 54.29% and 86.72%, respectively, and the detection rate of Deep EMD-PCA method is 91.36%, so we can obtain that the detection rate of Deep EMD-PCA method is significantly increased. This is because the method can retain more variance information and weak fault features can be extracted quickly. The false detection rate of the Deep EMD-PCA method is significantly reduced. On the other hand, from the comparison of the detection delay, Deep EMD-PCA can be detected from the beginning of the fault. So, the Deep EMD-PCA method has good fault detection performance.

5. Conclusions

In this paper, a novel incipient fault detection method based on Deep EMD-PCA is proposed. The method uses EMD-PCA to decompose the vibration signal and divide the signal into components of different frequency segments from high to low, reduce the data dimension, and realize fault detection. Then, we divide the dataset into multiple subdatasets for analysis, so that the weak fault information in the system is analyzed and incipient fault detection is realized. It is proved by theoretical analysis that this method has good performance in incipient fault detection. The method has the following advantages:

(1) Deep EMD-PCA method can extract weak fault features compared with EMD-PCA method and PCA-SVM method through multi-data processing layer, which is helpful for incipient fault detection

(2) It establishes accurate data models to improve incipient fault detection capability

(3) According to the experimental results, we can indicate that the detection rate of Deep EMD-PCA is about 85%, and the failure detection delay time is almost zero. Sensitive to weak fault features, we can find incipient fault more accurately

The incipient fault detection method based on Deep EMD-PCA effectively improves the accuracy and timeliness of fault detection under actual working conditions and has good practical application value.

Data Availability

The data used to support the findings of this study are included within the article.

Conflicts of Interest

The authors declare that there are no conflicts of interest regarding the publication of this paper.

Acknowledgments

This research was funded by the National Science Foundation of China under grant numbers 52075348, 51705341, and 51905357 and the Natural Science Foundation of Liaoning Province (No. 2019-ZD-0654).

References

[1] C. Q. Shen, Y. M. Qi, J. Wang, G. G. Gai, and Z. K. Zhu, "An automatic and robust features learning method for rotating machinery fault diagnosis based on contractive autoencoder," *Engineering Applications of Artificial Intelligence*, vol. 76, pp. 170–184, 2018.

[2] H. T. Shi, X. T. Bai, and K. Zhang, "Influence of uneven loading condition on the sound radiation of starved lubricated full ceramic ball bearings," *Journal of Sound and Vibration*, vol. 461, Article ID 114910, 2019.

[3] Y. Li, Y. Yang, X. Wang, B. Liu, and X. Liang, "Early fault diagnosis of rolling bearings based on hierarchical symbol dynamic entropy and binary tree support vector machine," *Journal of Sound and Vibration*, vol. 428, pp. 72–86, 2018.

[4] D. Barater, J. Arellano-Padilla, and C. Gerada, "Incipient fault diagnosis in ultrareliable electrical machines," *IEEE Transactions on Industry Applications*, vol. 53, no. 3, pp. 2906–2914, 2017.

[5] H. T. Shi and X. T. Bai, "Model-based uneven loading condition monitoring of full ceramic ball bearings in starved lubrication," *Mechanical Systems and Signal Processing*, vol. 139, Article ID 106583, 2020.

[6] H. Li, Y. Niu, Z. Li, Z. Xu, and Q. Han, "Modeling of amplitude-dependent damping characteristics of fiber reinforced composite thin plate," *Applied Mathematical Modelling*, vol. 80, pp. 394–407, 2020.

[7] M. S. Li, Y. Da, Z. Chen, K. Xiahou, T. Ji, and Q. H. Wu, "A data-driven residual-based method for fault diagnosis and isolation in wind turbines," *IEEE Transactions on Sustainable Energy*, vol. 10, no. 2, pp. 895–904, 2018.

[8] H. T. Shi, Y. Y. Li, X. T. Bai et al., "Investigation of the orbit-spinning behaviors of the outer ring in a full ceramic ball bearing-steel pedestal system in wide temperature ranges," *Mechanical Systems and Signal Processing*, vol. 149, Article ID 107317, 2020.

[9] L. L. Cui, X. Wang, H. Q. Wang, and J. F. Ma, "Research on remaining useful life prediction of rolling element bearings based on time-varying Kalman filter," *IEEE Transactions on Instrumentation and Measurement*, vol. 69, no. 6, pp. 2858–2867, 2019.

[10] L. Liu, Y. J. Liu, D. Li, S. Tong, and Z. Wang, "Barrier Lyapunov function-based adaptive fuzzy FTC for switched systems and its applications to resistance-inductance-capacitance circuit system," *IEEE Transactions on Cybernetics*, vol. 50, no. 8, pp. 3491–3502, 2019.

[11] X. Jiang, C. Shen, J. Shi, and Z. Zhu, "Initial center frequency-guided VMD for fault diagnosis of rotating machines," *Journal of Sound and Vibration*, vol. 435, pp. 36–55, 2018.

[12] Q. C. Jiang, X. F. Yan, and B. Huang, "Review and perspectives of data-driven distributed monitoring for industrial plant-wide processes," *Industrial & Engineering Chemistry Research*, vol. 58, no. 29, pp. 11899–11911, 2019.

[13] Y. Qi, C. Shen, D. Wang, J. Shi, X. Jiang, and Z. Zhu, "Stacked sparse autoencoder-based deep network for fault diagnosis of rotating machinery," *IEEE Access*, vol. 5, pp. 15066–15079, 2017.

[14] G. Li, G. Tang, G. Luo, and H. Wang, "Underdetermined blind separation of bearing faults in hyperplane space with variational mode decomposition," *Mechanical Systems and Signal Processing*, vol. 120, pp. 83–97, 2019.

[15] D. Wang, X. Zhao, L.-L. Kou, Y. Qin, Y. Zhao, and K.-L. Tsui, "A simple and fast guideline for generating enhanced/squared envelope spectra from spectral coherence for bearing fault diagnosis," *Mechanical Systems and Signal Processing*, vol. 122, pp. 754–768, 2019.

[16] W. Deng, H. Liu, J. Xu, H. Zhao, and Y. Song, "An improved quantum-inspired differential evolution algorithm for deep belief network," *IEEE Transactions on Instrumentation and Measurement*, vol. 69, no. 10, pp. 7319–7327, 2020.

[17] D. Wang and T. Kwok-Leung, "Dynamic Bayesian wavelet transform: new methodology for extraction of repetitive transients," *Mechanical Systems and Signal Processing*, vol. 88, pp. 137–144, 2017.

[18] W. You, C. Q. Shen, D. Wang, L. Chen, and X. X. Jiang, "An intelligent deep feature learning method with improved activation functions for machine fault diagnosis," *IEEE Access*, vol. 8, pp. 1975–1985, 2020.

[19] Y. Liu, Y. L. Zhao, J. T. Li, H. Ma, Q. Yang, and X. X. Yan, "Application of weighted contribution rate of nonlinear output frequency response functions to rotor rub-impact," *Mechanical Systems and Signal Processing*, vol. 136, Article ID 106518, 2020.

[20] L. Tang, D. Ma, and J. Zhao, "Adaptive neural control for switched non-linear systems with multiple tracking error constraints," *IET Signal Processing*, vol. 13, no. 3, pp. 330–337, 2018.

[21] B. Luo, H. T. Wang, H. Q. Liu, B. Li, and F. Peng, "Early fault detection of machine tools based on deep learning and dynamic identification," *IEEE Transactions on Industrial Electronics*, vol. 66, no. 1, pp. 509–518, 2018.

[22] H. Shi, L. Guo, S. Tan, and X. Bai, "Rolling bearing initial fault detection using long short-term memory recurrent network," *IEEE Access*, vol. 7, pp. 171559–171569, 2019.

[23] N. V. P. Kuraku, Y. He, and M. Ali, "Fault diagnosis of open circuit multiple IGBT's using PPCA-SVM in single phase five-level voltage controlled H-Bridge MLI," *IEEJ Journal of Industry Applications*, vol. 9, no. 1, pp. 61–72, 2020.

[24] H. Wu and J. Zhao, "Deep convolutional neural network model based chemical process fault diagnosis," *Computers & Chemical Engineering*, vol. 115, pp. 185–197, 2018.

[25] H. T. Zhang, H. X. Chen, and Y. B. Guo, "Sensor fault detection and diagnosis for a water source heat pump air-conditioning system based on PCA and preprocessed by combined clustering," *Applied Thermal Engineering*, vol. 160, Article ID 114098, 2019.

[26] S. Ji, H. Cao, J. Zhao, Y. Pan, and E. Jiang, "Soft abrasive flow polishing based on the cavitation effect," *The International Journal of Advanced Manufacturing Technology*, vol. 101, no. 5-8, pp. 1865–1878, 2019.

[27] K. Yu, T. R. Lin, H. Ma, X. Li, and X. Li, "A multi-stage semi-supervised learning approach for intelligent fault diagnosis of rolling bearing using data augmentation and metric learning," *Mechanical Systems and Signal Processing*, vol. 146, Article ID 107043, 2021.

[28] L. Tang and D. Li, "Time-varying barrier Lyapunov function based adaptive neural controller design for nonlinear pure-feedback systems with unknown hysteresis," *International Journal of Control, Automation and Systems*, vol. 17, no. 7, pp. 1642–1654, 2019.

[29] H. Chen, B. Jiang, N. Lu, and Z. Mao, "Deep PCA based real-time incipient fault detection and diagnosis methodology for electrical drive in high-speed trains," *IEEE Transactions on Vehicular Technology*, vol. 67, no. 6, pp. 4819–4830, 2018.

[30] X. Mao, J. Zhang, M. Lv, G. Shen, and J. Yang, "Realising the decomposition of a multi-frequency signal under the coloured noise background by the adaptive stochastic resonance in the non-linear system with periodic potential," *IET Signal Processing*, vol. 12, no. 7, pp. 930–936, 2018.